JOURNAL OF AIRCRAFT
Vol. 29, No. 4, July–Aug. 1992

Unsteady Aerodynamics of a Wortmann Wing at Low Reynolds Numbers

H.-T. Liu*
QUEST Integrated, Inc., Kent, Washington 98032

The unsteady effects of turbulence and gusts on the performance of a full-scale Wortmann FX 63-137 wing for remotely piloted vehicle applications were studied by conducting experiments in the atmospheric boundary layer. The wing, which had an aspect ratio of 6, was mounted on an instrumented truck equipped for force/moment and wind measurements. The vehicle remained stationary, and the wing was aligned with the prevailing wind. The wing experienced predominantly a plunging rather than a pitching motion, together with sweeping and longitudinal oscillations, due to the unsteady three-dimensional wind field. The chord Reynolds number ranged from 250,000 to 450,000, and the turbulence intensity ranged from 8% to about 20%. From the spectra of the wind components, the reduced frequencies experienced by the wing may be up to 0.1 or higher, indicating that unsteady effects are important. The results show significant lift overshoot, resulting in an increase in the maximum lift coefficient and stall angle. The aerodynamic coefficients do not show pronounced hysteresis loops. A significant reduction of the minimum drag coefficient was also observed, consistent with the theory of a rigid-wing plate undergoing plunging oscillation. It was concluded that the fluctuating wind field significantly improved the wing's maneuverability and endurance.

Introduction

ONE of the least understood factors in the performance of low-altitude, low-Reynolds-number remotely piloted vehicles (RPVs), man-powered airplanes, and hang gliders is the effect of atmospheric unsteadiness such as turbulence and gusts. Many qualitative descriptions of how such unsteadiness affects performance have been given by operators of low-Reynolds-number (LRN) vehicles. In the atmospheric boundary layer above the ground or ocean surface, the characteristics of the flowfield vary not only with the atmospheric conditions, but also with surface conditions such as stability, terrain topography, and sea states. Therefore, LRN vehicles are expected to encounter atmospheric turbulence and gusts at a wide range of temporal and spatial scales.

Recently, the field of unsteady aerodynamics has become an important research topic. Until now, however, studies of unsteady flows over lifting surfaces have been confined mainly to pitching and plunging airfoils,[1,2] due to the need to better understand the performance of helicopter rotors. Limited studies have also been conducted to investigate unsteady motions in the streamwise direction and at various oblique angles relative to the oncoming flow.[3] Because of the complexity of the problem, only minimal effort has been directed to the study of the interaction between an airfoil/wing and a gust field.[4] Most of the above studies assume a two-dimensional flow, although three-dimensionality is usually present and has been shown to have significant effects on dynamic stall.[5]

An environmental aerodynamic test system (EATS) has been developed specifically to study the effects of atmospheric disturbances on the performance of a full-scale wing for RPV applications.[6,7] This system includes an instrumented truck as the mobile platform, a boom-mounted full-scale wing, and an aerodynamic balance mounted inside the wing. The wing has the profile of a Wortmann FX 63-137 airfoil (smoothed by Eppler) with a span of 3.66 m and a chord of 0.61 m (i.e., an aspect ratio of 6). The airfoil was chosen because it performs reasonably well for a chord Reynolds number (R_c) as low as 100,000–150,000.[8] Also, sufficiently accurate wind-tunnel data are available for steady conditions and can be used as baseline data for evaluating the wing's performance in the atmospheric boundary layer.[9,10] A "park mode" configuration was used for the EATS experiment; that is, the vehicle remained stationary and the wing was directed into the prevailing wind in open fields. These tests were conducted at the Ellensburg Airport in Ellensburg, Washington, to take advantage of the favorable wind conditions and terrain at this site. (During the windy season in late spring and early summer, the prevailing westerly wind of up to 20 m/s often persists for days, and the terrain is very flat for miles upwind of the airport toward the foothills of the Cascade Mountains.)

Received Feb. 14, 1991; revision received May 16, 1991; accepted for publication May 16, 1991.

*Principal Scientist, Applied Physics Division (formerly Flow Research, Inc.), 21414 68th Avenue South. Member AIAA.

Background

Steady Aerodynamics

Under steady conditions, wind-tunnel experiments at the University of Notre Dame[9] and at Virginia Polytechnic Institute (VPI)[10] showed that the lift coefficient of the Wortmann wing does not vary linearly with the angle of attack in the well-known linear lift regime for $R_c < 100{,}000$. The linear trend reappears for $R_c > 150{,}000$. The lift coefficient increases while the drag coefficient decreases with the aspect ratio of the wing. In the Notre Dame experiments, the maximum value of the lift coefficient of the Wortmann wing (aspect ratio = 5.4) at $R_c = 200{,}000$ was estimated to be about 1.5 at 18 deg. Both the lift coefficient (C_L) vs angle of attack (α_0) and the drag coefficient (C_D) vs α_0 curves showed distinctive hysteresis loops. Increasing the Reynolds number or reducing the aspect ratio tends to reduce the size of the hysteresis loops.

The performance characteristics of the Wortmann wing in a steady airstream have been investigated in several wind tunnel facilities.[8,10,11] At low Reynolds numbers ($R_c \simeq 80{,}000$ to 300,000), discrepancies were found among the wind-tunnel results for the same wing models due to differences in environmental conditions (freestream turbulence intensity and spectra, tunnel acoustics, and mechanical vibration) and in measurement techniques (force balance, wake traverse, and surface pressure integration), as discussed in Refs. 8, 9, and 12. For example, the results measured at the VPI facility[10] show features similar to those measured at the Notre Dame

facility,[9] but with some differences in the values of C_L and C_D as a function of α_0 and in the shape of the hysteresis loops.

The performance of a wing is very sensitive to external disturbances at or near static stall, especially for Reynolds numbers below 200,000. High levels of freestream turbulence, acoustic noise, and mechanical vibration may significantly reduce the hysteresis loops.[12,13] In fact, a statically stalled wing can be unstalled simply by knocking on the wind tunnel wall or by creating an upstream acoustic disturbance. Note that not all of the differences can be attributed to freestream disturbances. Imperfections in the model, surface roughness, or an increase in the Reynolds number can produce results identical to those achieved with freestream disturbances. At the 1985 and 1986 Conferences on Low Reynolds Number Airfoil Aerodynamics held at the University of Notre Dame and the Royal Aeronautic Society, it was generally agreed that the model and environmental conditions for wind-tunnel tests should be specified as completely and accurately as possible. In presenting the freestream turbulence, for example, the turbulence intensity, acoustic level, and their spectra should be specified.

Unsteady Phenomena

The unsteadiness of the wind field effectively causes the Wortmann wing to experience pitching/plunging motions, which have been found to have significant effects on the aerodynamics. As will be seen later, the power spectra of the wind field show that the spectral densities of the U and W velocity components beyond 2 Hz are at least two decades below the spectral peak. Under the influence of the low-frequency fluctuating wind components, the wing is predominantly subjected to a plunging rather than a pitching motion.

Pitching/Plunging Motions

When an airfoil undergoes oscillatory motions, i.e., pitching or plunging, several dramatic phenomena take place that deviate greatly from the static situation. As discussed by Ho[14] and demonstrated by McCroskey,[15] the excursion of the aerodynamic properties from that of the static case depends on the operational parameters of the unsteady motion. The difference can be very pronounced if a large separation vortex occurs at the leading edge. When the angle of attack oscillates around a mean value α_0 near or greater than the static stall angle, the maximum values of the lift, drag, and pitching-moment coefficients can greatly exceed their static counterparts. The higher value in the lift coefficient is generally referred to as the "lift overshoot." Such increases in C_L, C_D, and the pitching coefficient, C_M, cannot be reproduced even qualitatively by neglecting the unsteady motion of the airfoil. On the other hand, large hysteresis develops in the aerodynamic forces and moments with respect to the instantaneous angle. The above process is referred to as dynamic stall, which is intimately related to unsteady separation of the flow around the oscillating airfoil.

McCroskey[1,15] found that the primary parameter that determines the degree of separation is the maximum angle of attack. He classified the viscous-inviscid interaction for an oscillating airfoil into three important regimes: stall onset, light stall, and deep stall. Stall onset is the limiting case of the maximum unsteady lift that can be obtained with no significant penalty in pitching moment and drag. It represents a measure of the maximum useful lift that a given airfoil/wing can deliver if drag rise and moment stall are to be avoided. Further increases in the angle of attack produce dynamic stall, which is characterized by large phase lags and hysteresis in the separation and reattachment of the viscous flow. In light stall, the scale of the viscous-inviscid interaction remains on the order of the airfoil thickness; changes in the behavior of the oscillating airfoil response are closely related to the separation characteristics of the boundary layer and its dependence on the airfoil shape, reduced frequency, maximum incidence, and Mach number. As the maximum incidence increases to values well in excess of the static stall angle, the flow over the airfoil is in the deep stall regime. A strong, vortex-like disturbance forms in the leading edge region, sheds from the boundary layer, and moves downwind over the upper surface of the airfoil, producing large amounts of hysteresis in C_L, C_D, and C_M. The scale of the viscous interaction zone is large, and the thickness of the viscous layer is on the order of an airfoil chord. If the Mach number is low, these features are relatively insensitive to the airfoil shape, airfoil motion, and Reynolds number.

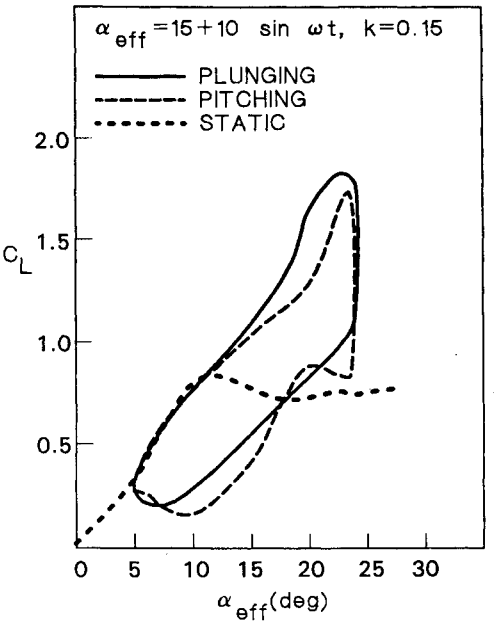

Fig. 1 Lift overshoot resulting from pitching and plunging motions of an airfoil.[3]

In the case of a plunging airfoil, a similar response in deep stall has been shown by Maresca et al.,[3] but significant differences in light stall have been reported by Carta[16] and Chen.[2] Their results show that, at high load conditions, the normal force for equivalent pitch (due to plunging) has higher slopes than that for true pitch, as demonstrated in Fig. 1. There appears to be a major difference in the way in which stall flow breakdown occurs for these two unsteady motions. For true pitch, a conventional leading edge stall cell or vortex that propagates downstream along the chord is formed. However, the stall cell for equivalent pitch is not well-organized and, if it occurs, has no orderly downstream propagation. For a range of mean (equivalent) angles of attack of around 12–14 deg, Chen[2] observed from surface pressure measurements that a low-pressure zone developed near the leading edge due to the passage of a vortex-like disturbance. This disturbance moves downstream over the airfoil surface at about 20–30% of the average freestream speed, which is lower than that of the pitching case as observed by McCroskey.[17] The vortex does not have a strong vortex peak, and the low-pressure zone formed on the upper surface is elongated. The vortex penetration is also less severe, as in the case of a pitching airfoil.[16] Consequently, a high lift coefficient could be sustained for a relatively long period of time after passing the static stall angle, mainly due to the elongated low-pressure disturbance zone and its slow convection speed on the upper surface of the airfoil.

Thrust Generation

In the wakes of an airfoil oscillating at amplitudes of 2 and 4 deg, Koochesfahani[18] has demonstrated that the vortex street changes from a wake-like to a jet-like pattern as the reduced frequency increases beyond a few degrees, depending on the

amplitude. In other words, the usual wake profile with a velocity deficit (i.e., an airfoil with drag) can be transformed into a wake with a velocity excess (i.e., an airfoil with thrust) above the critical frequency. In the frequency range between zero and the critical value, the drag tends to be lower than that of the airfoil at its mean angle of attack (set at zero) with no oscillation. Similar findings were reported by Wu and Singh,[19] who investigated the unsteady aerodynamics of an articulate body consisting of an oscillating posterior plate hinged to a fixed plate. During the major part of the oscillating cycle, the force is negative, indicating that the articulate body experiences a thrust.

It should be noted that the jet-like vortex pattern corresponding to a thrust-generating flat plate in plunging oscillation is a well-known phenomenon described by Von Karman and Burgers.[20] Wu[21] has investigated the hydrodynamic efficiency (the ratio of the product of the thrust and the wind speed to the total power required) of a rigid-plate wing undergoing heaving (plunging) and pitching motion. He has shown that the hydrodynamic efficiency of the wing undergoing heaving alone is consistently higher than that of the wing undergoing pitching alone. It is evident that significant drag reduction may be achieved by pitching or plunging a wing at small angles of attack, with the latter being more efficient than the former for all reduced frequencies but particularly at low reduced frequencies. Net propulsion may result as the thrust exceeds the drag force.

Longitudinal Oscillations

The studies of Maresca et al.[3] also established the existence of the vortex-shedding phenomenon and strong hysteresis effects due to translational oscillations in the streamwise direction and at various oblique angles relative to the oncoming flow. In the longitudinal oscillation case, for example, unsteady effects were found to be strong enough to unstall the airfoil during part of the cycle, even when the incidence was considerably above the maximum static angle.

Three-Dimensional Effects

Despite the fact that almost all practical lifting devices develop or encounter three-dimensional flow, common engineering practice is to use the so-called strip theory and the two-dimensional stall characteristics outlined above. This is done partly for simplicity and partly because of the lack of information about three-dimensional flow.

St. Hilaire et al.[5] examined the effect of sweeping an oscillating wing model at an angle λ with respect to the freestream. Their results show that sweep tends to delay the onset of dynamic stall and to reduce the rate of change of C_L and C_M as stall begins. It also reduces somewhat the magnitude of the hysteresis loops.

The above description is qualitatively applicable to the present situation, except that the laboratory experiments were limited to sinusoidal oscillations of a single frequency, whereas the wind components in the present experiments had a wide range of frequencies. However, it was anticipated that the results of the present experiments would differ from those wind-tunnel results obtained under steady flow conditions.

Environmental Aerodynamic Test System

A detailed description of the EATS has been given elsewhere.[6] Several modifications to improve the performance of the EATS have been implemented after many series of full-scale tests. In this section, an updated description of the EATS is presented.

Aerodynamic Balance

A detailed description of the original aerodynamic balance is given elsewhere.[6] A slight modification of the original design has been made to strengthen the balance to resist motion in the yaw direction.[7] As a result, the side-force cells were decommissioned; the side force and yawing moment can no longer be measured. Recalibration shows that the above modification reduces the sensitivity of the chord-force cell by only 1.5%, without affecting that of the normal-force cells.

The dynamic response of the load cells is very high, according to specifications provided by the manufacturer. The maximum axial displacement of the load cell under the maximum loading is less than 0.001 cm. Because the balance is rigidly assembled, no significant degradation in the dynamic response of the balance as a whole from that of the individual load cells is anticipated. Therefore, the dynamic response of the EATS is limited by the relatively low response of the propeller anemometer, which has a distance constant of 0.8 m (63% recovery). For a wind speed of 10 m/s, the corresponding time constant, t_c, is 0.08 s. The frequency response at -3 dB down is therefore

$$f_{-3\text{dB}} \simeq 1/(2\pi t_c) = 2 \text{ Hz} \quad (1)$$

To match the response of the anemometer, the output signals of the load cells are low-passed at about 4–5 Hz. A special setup was assembled to test the dynamic response of the balance. This setup includes a cam that displaces a 9-kg weight hanging on the wing at the trailing edge. As the cam is rotated, the wing experiences periodic loading. The ratio of the peak-to-peak lift and drag forces, in response to the periodic loading for a range of rotational frequencies, remains flat up to 1 Hz and falls off to about 0.6 at 5 Hz, which is the -3 dB point of the low-pass filter.

Angle Measurements

Two mini-clinometers were used to set and monitor the angle of attack of the wing and the leveling of the wing in the crosswind direction. These instruments have excellent temperature stability, with null and scale factor temperature coefficients of 0.008 deg/°C and 0.05 deg/°C, respectively. They have an overall repeatability of $\pm 0.1°$, and their time constant is about 3 s, with a settling time of 15 s. One of the clinometers was mounted on the dividing head and the other on its base, on top of the supporting steel beam. Leveling of the EATS in the horizontal plane was achieved by jacking up the vehicle at three points under the main body frame and then bracing the EATS on both sides with two thick-walled steel pipes (3.8 cm OD). The angle of attack was then adjusted by rotating the dividing head according to the output reading of the clinometer. During each run, both the angle of attack and the crosswind level were monitored. A third clinometer was mounted on the anemometer to monitor its alignment with respect to the wing orientation.

Setup for Force/Moment Measurements

For each angle of attack, a series of about 10 runs was conducted. Once the angle of attack was set, the gain and the zero offset of the load cells were then adjusted to optimize the range of force/moment measurements according to the expected wind conditions. The reference voltage outputs of the load cells and anemometers under no-wind conditions were recorded before or after each series of runs. The reference runs were conducted in very calm conditions inside a closed hanger at the Ellensburg Airport.

After the reference runs, the EATS was moved to the open field, the wing was aligned to the prevailing wind direction, and the system was set up for the runs according to the following procedure: 1) jack up, brace, and level the truck; 2) check the alignment of the wing with the prevailing wind (the V propeller should oscillate around zero wind speed); 3) check and fine-adjust the angle of attack of the wing and the alignment of the anemometer; 4) recheck the gain and offset of the load cells, resetting them if necessary (post reference runs were made if gain and offset were reset); 5) load computer programs and record data; and 6) if necessary, realign the wing with the prevailing wind and repeat steps 1 through 5.

Data Acquisition and Analysis

A description of the various sensors and electronics, the analog-to-digital interface, and the microcomputer and peripherals has been given elsewhere.[6] The software and procedures for data acquisition and the software and hardware for data analysis have also been presented in another paper.[7] A brief summary of the software and hardware is given here.

Software for Data Acquisition

To maximize the data rate, the program for data acquisition was written in assembly language. This program contains all the instructions for retrieving the 12-bit numbers from an analog input system and storing them in the memory of the computer. A second BASIC program was written to input the run parameters, such as the number of channels, sampling frequency, number of data points, specific data channels, and the gain for each channel to be sampled. During the execution of the data acquisition program, the BASIC program is called, and the data stored in the memory are then transferred to a $5\frac{1}{4}$-in. floppy disk for long-term storage. The maximum sampling rate is about 12,000 samples/s, and the maximum number of data points is about 12,000. For example, for a channel number of 6, the maximum sampling rate for each channel is 2000 Hz and the maximum number of samples per channel is 2000.

Software/Hardware for Data Analysis

Part of the data analysis was conducted using the microcomputer. A BASIC program was developed to convert the raw data into physical units in terms of the lift (L), the drag (D), the pitching moment (M), the three velocity components (U, V, W) of the wind field, and the vertical acceleration (A). The lift and drag are derived from the following formulas:

$$L = F_N \cos \alpha' - F_C \sin \alpha' \tag{2}$$

$$D = F_N \sin \alpha' + F_C \cos \alpha' \tag{3}$$

where F_N and F_C are the normal and chord forces in the balance coordinate, and α' is the angle of attack of the balance with respect to the local wind field, or

$$\alpha' = \alpha + \arctan(\overline{W}/\overline{U}) \tag{4}$$

with $\overline{W}$ and $\overline{U}$ being the time averages of W and U, and α being the angle of attack of the balance with respect to the horizontal. The angle of attack of the wing α_0 is

$$\alpha_0 = \alpha' + 4 \text{ deg} \tag{5}$$

The pitching moment referenced to the $\frac{1}{4}$-chord may be estimated from

$$M = [(F_N)_1 + (F_N)_2]x_1 - (F_N)_3 x_2 + F_C x_3 \tag{6}$$

where $(F_N)_1$, $(F_N)_2$, and $(F_N)_3$ are the force components measured by the three normal-force load cells, and x_1, x_2, and x_3 are the displacements of the cells from the $\frac{1}{4}$-chord point.

Based on these quantities, the lift, drag, and pitching-moment coefficients (C_L, C_D, and C_M) may be derived by dividing Eqs. (2) and (3) by $\frac{1}{2}\rho(\overline{U}^2 + \overline{W}^2)S$, and by dividing Eq. (6) by $\frac{1}{2}\rho(\overline{U}^2 + \overline{W}^2)SC$, respectively. Here, ρ is the density of air, S is the planform area of the wing, and C is the chord length.

Provision is also made to smooth the data by averaging the raw data over a short time period (0.25 s, 0.5 s, 1 s, 2 s, etc.) before calculating the forces, the moment, and their coefficients. Mean and root-mean-square values of the physical quantities are estimated from a relatively large section of the time series recorded on disks. The results are stored in an ASCII file on floppy disks. This file may be transferred to a portable computer for further analysis and graphic display, using BASIC programs and commercially available software.

Results and Discussion

In this section, the results of one of the series of field experiments conducted at the Ellensburg Airport are presented. Additional results are reported elsewhere.[7] Only the time-averaged aerodynamic parameters are presented here. The instantaneous results and corresponding spectra information are given in another report.[22] The data set consists of a total of 76 runs. The mean wind speed and turbulence intensity range from 6.3–11.5 m/s and from 8–20%, respectively.

Wind Characteristics

Figure 2 shows a typical time series of the three velocity components U, V, and W, with the W component shifted by -6 m/s. The abscissa and ordinate are the time in seconds and the velocity components in meters per second, respectively. The raw data (1800 points) were recorded at a sampling rate of 6 Hz, and only the 3-point averages, or the equivalent of a 2-Hz sampling rate, are presented in the figure. The total sampling time is 5 min. The mean wind speed is 8.63 m/s, and the turbulence intensities u'/U and w'/U are 14 and 12%, respectively. From Fig. 2, it is found that the U and V components are comprised of low- and high-frequency fluctuations, whereas the W component shows insignificant low-frequency fluctuations. During this time period, the prevailing wind direction meanders slowly, as demonstrated by the V-component time series. For most runs, the total sampling times were either 90 s (with a sampling rate of 20 Hz) or 20

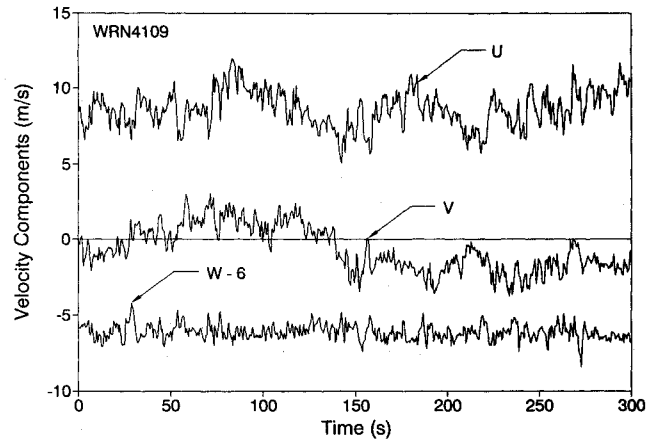

Fig. 2 Time series of wind components (0.5-s averages) measured at the Ellensburg Airport with record length of 5 min.

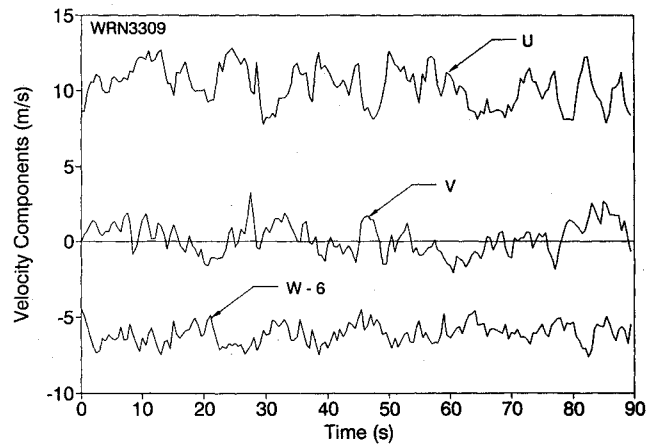

Fig. 3 Time series of wind components (0.5-s averages) measured at the Ellensburg Airport with record length of 1.5 min.

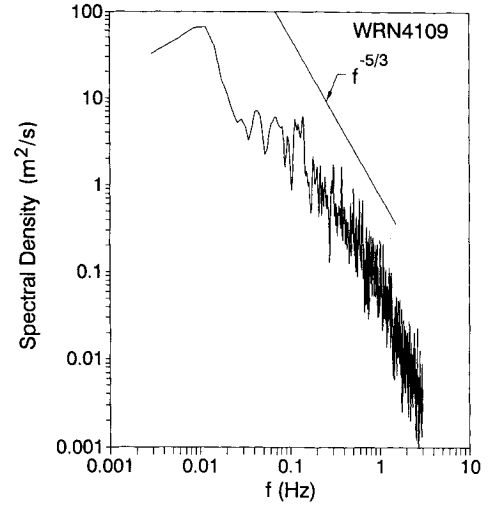

Fig. 4 Power spectra of U and W components of the wind field corresponding to the time series in Fig. 1.

s (with a sampling rate of 80 Hz). For the short runs, it was possible to have a better selection of the constancy of the mean wind speed and direction, as illustrated in Fig. 3.

The power spectra of the U and W components corresponding to Fig. 2 are shown in Fig. 4. The spectra were estimated by performing direct fast Fourier transforms of the velocity time series, with the use of a cosine window. Since the maximum number of data points is 1800, zeros were added to either side of the time series to make a total of 2048 data points. The abscissa and ordinate are the logarithmic frequency in hertz and the spectral density in meters-squared per second, respectively. The shapes of the two spectra are quite different. The U spectrum (Fig. 4a) peaks at about 0.01 Hz, whereas the W spectrum (Fig. 4b) has a relatively broad peak for $f < 0.5$ Hz. The ratio of the two spectral peaks, $SU(f_0)/SW(f_0)$, is about 15, where f_0 is the dominant frequency. The U spectrum shows a $-5/3$ power regime between $0.1 < f < 1$ Hz. Beyond 1 Hz, the spectrum falls off as f^{-3}. Part of the reason for this steeper falloff is the slow response of the anemometers, whose -3 dB point is at about 2 Hz. The W spectrum does not show an extensive $-5/3$ regime as the result of the reduction in the frequency response of the W propeller, $f_{-3dB} \simeq 0.5$ Hz, due to the low mean W value (note that the anemometer was tilted at 15 deg to improve the frequency response of the propeller). It should be pointed out that the W spectral density at $f = 0.5$ Hz is about 1 decade lower than that of the spectral peak.

Force/Moment Measurements

Figure 5 displays the time series of the lift, drag, and pitching moment corresponding to the wind conditions shown in Fig. 3. The dimensions for the force and moment are Newtons and Newton-meters. For this run, the mean geometric angle was 13.5 deg, with -0.5 deg attributed to a small negative mean W component. A comparison of Figs. 3 and 5 indicates that the lift and drag correlate well with the U and W components, respectively. The pitching moment also correlates well with the W component.

In Figs. 6 through 8, the lift, drag, and pitching-moment coefficients are presented as a function of the angle of attack. These results were derived from the full-scale (FS) measurements conducted at the Ellensburg Airport. There were a total of 76 runs with the mean angle of attack ranging from -18 to 30 deg. The average wind speed ranged from 6.3 to 11.5 m/s, which resulted in a chord Reynolds number from 250,000 to 450,000. In the figures, the circles ($350{,}000 < R_c < 450{,}000$) and the triangles ($250{,}000 < R_c < 350{,}000$) are

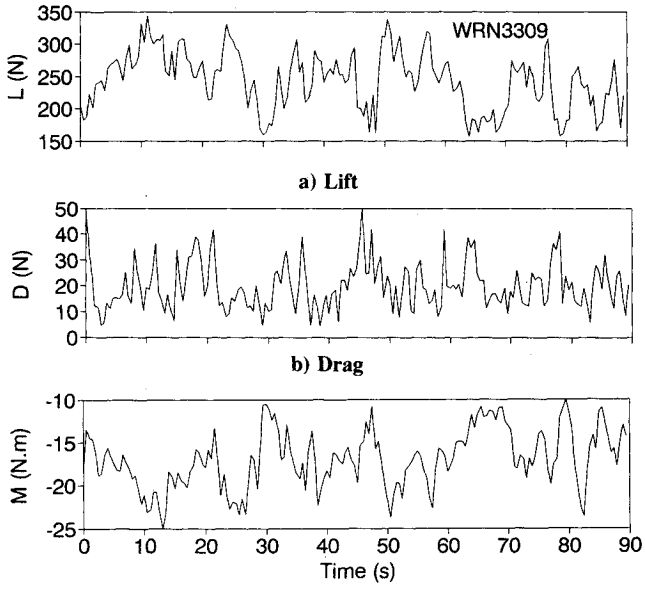

Fig. 5 Time series of lift, drag, and pitching moment (0.5-s averages). The corresponding wind conditions are shown in Fig. 2.

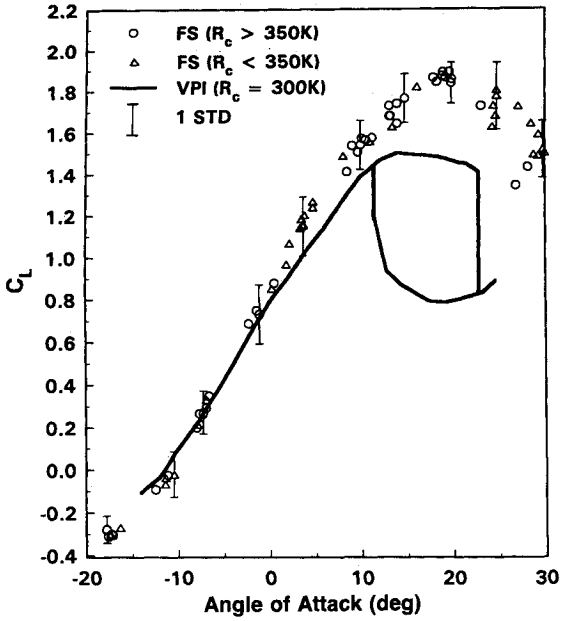

Fig. 6 Measurements of lift coefficients. The FS measurements correspond to the mean values of the 2-Hz data.

used to plot the long-time averages of the 2-Hz data. To properly interpret the results, it must be kept in mind that the experiments were conducted in the atmospheric boundary layer, not in a wind tunnel in which the flow is regulated carefully. As pointed out earlier, the wind is turbulent, with an intensity ranging from 8 to 20%. The coefficients have a fluctuating component that is one of the real physical properties of the data and that must be distinguished from the data scatter, which represents the uncertainty of the experiment.

In Figs. 6 through 8, the error bars indicate one standard deviation of the coefficients. The vertical spread represents the excursions in response to the fluctuating wind field for the corresponding runs with different ambient conditions. This spread must not be confused with data scatter in the conventional sense. In all fairness, the spread among the circles and triangles, which corresponds to the spread of the mean values of individual runs, is equivalent to the data scatter for the field measurements. Such a spread is surprisingly small, even far past the static stall angles of the steady counterparts, considering the unregulated nature of the wind field. Well-defined trends for the coefficients may be clearly established from the best-fit curves of the FS data. A comparison of the observed trends is made with those of wind-tunnel (WT) data obtained at VPI (solid curves), which have the highest R_c of 300,000[10] for a Wortmann wing with an aspect ratio of 6.

Within the range of Reynolds numbers from 250,000 to 450,000, the FS data display no discernible trend as a function of R_c. Despite the wide range of unsteadiness of the wind conditions, the long-time averages of the FS results are highly coherent and show a definite relationship to the angle of attack. The mean values show only a minimum spread except in the deep stall regime ($\alpha_0 > 20$ deg). The differences between the FS results and the steady WT data are considerable. Attempts have been made to differentiate the differences by attributing them to the unsteadiness of the wind field rather than to variances in the experimental configurations and measuring techniques; experimentalists have still not been able to identify differences due to the latter effects even between results obtained in different wind tunnels.

Figure 6 shows that the lift coefficients of the two data sets compare reasonably well for -10 deg $< \alpha_0 < 0$ deg. Outside this range, the lift curve of the FS results shows a consistently steeper slope. The WT results show a slight reduction in the slope of the lift curve for $\alpha_0 > 0$, whereas the FS results show an essentially constant slope up to $\alpha = 10$ deg. The maximum lift coefficient ($C_{L\max}$) is about 1.5 at 13 deg for the WT data, and 1.8 at 19 deg for the FS data. The ratios of $C_{L\max}$ and the corresponding angle of attack are 1.2 and 1.5, respectively, which is a significant improvement. Note that the $C_{L\max}$ for a Wortmann wing with a semi-aspect ratio of 2.7 obtained at the Notre Dame wind tunnel is 1.45 at 19 deg, but the C_L curve reaches a plateau at about 14 deg.

The observed "lift overshoot" is one of the distinctive features of the dynamic stall phenomenon for a wing undergoing unsteady motions at sufficiently high reduced frequency, defined as $k = \omega C/2U$ ($k > 0.05$). As demonstrated in Fig. 1, the overshoot is larger for a wing undergoing a plunging motion as compared to a pitching motion. From Fig. 4, it is found that the fluctuations of the wind components are reasonably energetic at frequencies up to 0.5 Hz, which translates into a range of reduced frequencies up to 0.11. The vertical spread of one standard deviation shown in the figure may be viewed as the statistical average of the hysteresis loop. Because the FS Wortmann wing was subject to a wide range of reduced frequencies rather than a single one, which is used in most WT tests, the present results would have more pronounced unsteady effects than most WT data reported in the literature.[1,14,15]

Figure 7 shows the C_D vs α_0 curve. The FS results again display a well-defined relationship between C_D and α_0 with a minimum spread for the mean values of C_D. The vertical

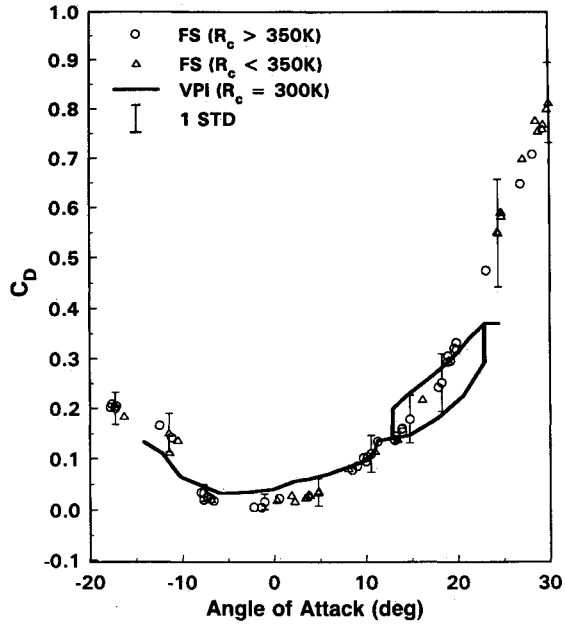

Fig. 7 Measurements of drag coefficients. The FS measurements correspond to the mean values of the 2-Hz data.

spread of one standard deviation, which is a measure of the unsteady effect, shows a large increase beyond 20 deg, which indicates the deep stall regime.

Comparison of the FS and WT data show significant differences. In the discussion below, the subscripts FS and WT are used to identify the full-scale data and the wind-tunnel data, respectively. The minimum drag coefficient for the full-scale data, $(C_{D\min})_{FS}$, is considerably lower than that for the wind-tunnel data, $(C_{D\min})_{WT}$, although it occurs at about the same range of α_0. As discussed earlier, the reduction in C_D at small angles of attack is attributed to the unsteadiness of the wind field, which translates into a plunging oscillation of the Wortmann wing. As estimated from Fig. 4, the maximum reduced frequency for the experiments is about 0.11. For a pure pitching motion, the reduction in the drag coefficient is not significant, based on the laboratory results of Koochesfahani.[18] When the superior hydrodynamic efficiency of the plunging oscillation is taken into consideration,[21] particularly at reduced frequencies below 1.781, the reduction in the drag coefficient may be substantial. The theory of thrust generation by a rigid-plate wing undergoing a heaving motion[21] supports the present finding of significant drag reduction at small angles, as shown in Fig. 7.

On either side of the minimum drag region, the slope of the $(C_D)_{FS}$ curve is steeper than that for $(C_D)_{WT}$; the larger increase in drag as α_0 increases or decreases is mainly attributed to the induced drag due to the higher unsteady lift in the FS cases. The FS data do not show the presence of a hysteresis loop in the same range of α_0 where a distinctive loop is observed for the WT data. Even in the deep stall regime where the standard deviation increases significantly, the spread of the mean values is small compared to the amplitude of the WT hysteresis loop. This indicates that the time-averaged FS lift and drag coefficients induced by the fluctuating wind in the deep stall regime do not have pronounced hysteresis loops, although the instantaneous excursion from their mean values could be large.[22]

Figure 8 shows the relation of C_M vs α_0. Note that the $(C_M)_{FS}$ is consistently below the $(C_M)_{WT}$ for the entire range of α_0 considered. The dramatic differences between the two sets of data are the absence of a pronounced hysteresis loop in the FS data set and the rapid falloff of $(C_M)_{FS}$ beyond the stall onset regime with $\alpha_0 < 13$ deg. By definition, the stall onset occurs at about 13 deg, at which $(C_L)_{FS}$ is noticeably higher than its steady counterpart, whereas $(C_D)_{FS}$ and $(C_M)_{FS}$ are

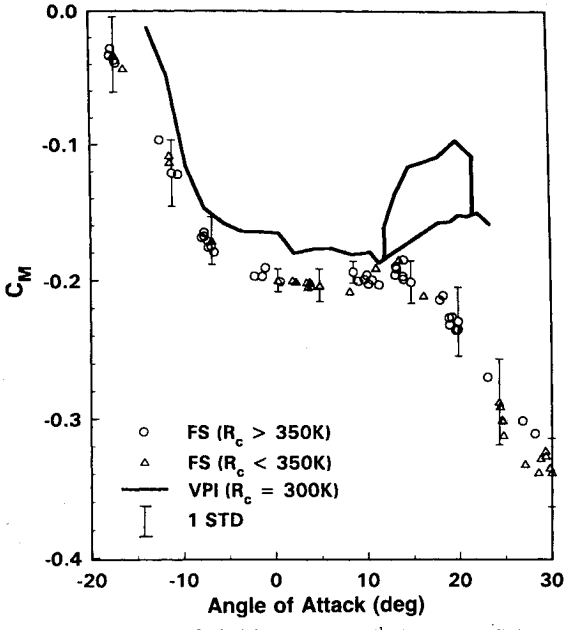

Fig. 8 Measurements of pitching-moment (¼ chord) coefficients. The FS measurements correspond to the mean values of the 2-Hz data.

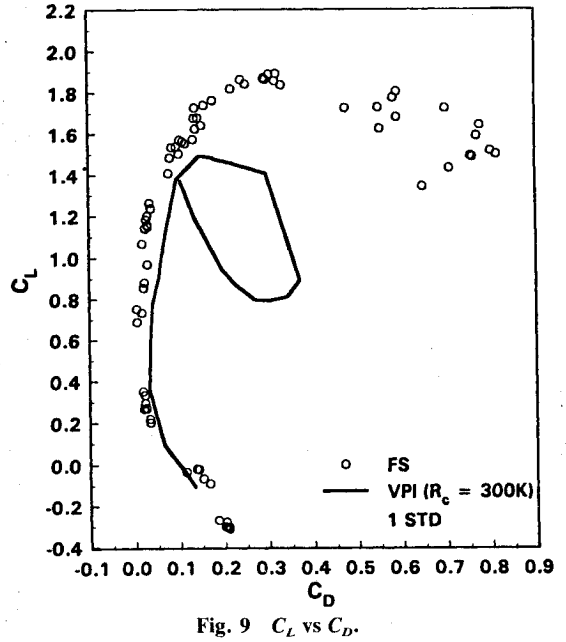

Fig. 9 C_L vs C_D.

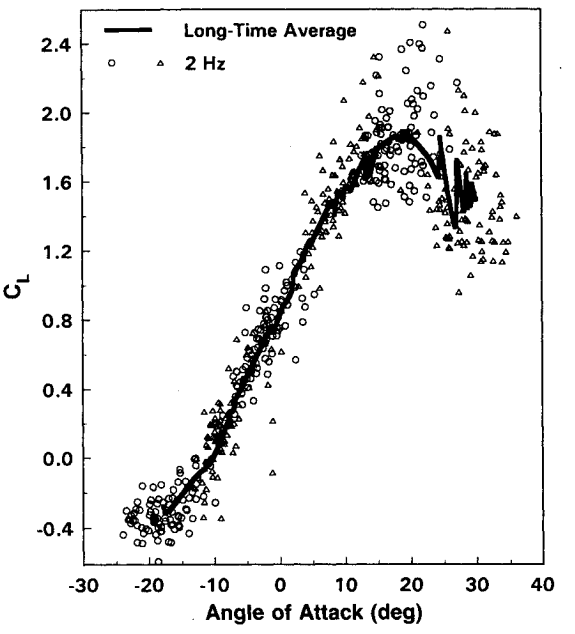

a) C_L

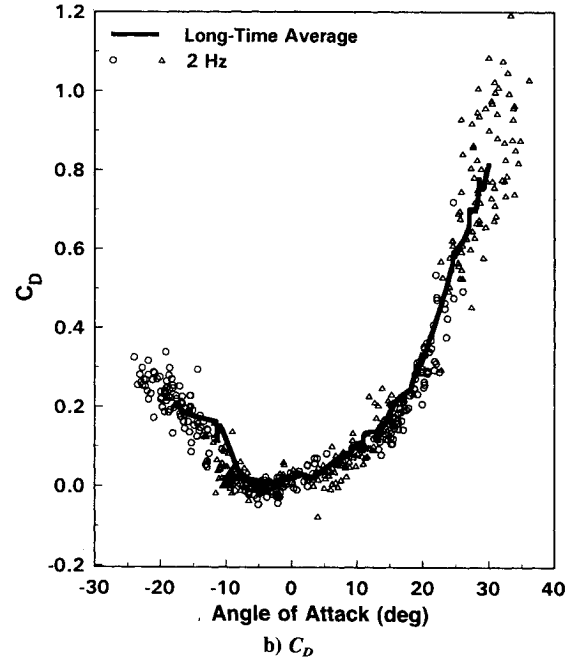

b) C_D

Fig. 10 Comparison of long-time (90 s) and short-time (0.5 s) averages of C_L and C_D.

comparable to those of the steady values. The opposite trend of $(C_M)_{FS}$ and $(C_M)_{WT}$ at large α_0 is mainly a result of the difference in the behavior of the $(C_L)_{FS}$ and $(C_L)_{WT}$, due to unsteady effects. It should be noted that $(C_M)_{FS}$ follows exactly the same trend of a plunging airfoil.[2,14,15]

Figure 9 is a plot of C_L vs C_D. For a given C_D, $(C_L)_{FS}$ is considerably higher than $(C_L)_{WT}$ except for small C_L. It is remarkable that the FS Wortmann wing performs so much better in the atmospheric boundary layer than does its WT counterpart under steady conditions. The effects of drag reduction at small angles of attack and of the dynamic stall at large angles induced by the unsteady wind field are the two main sources of the observed improvement.

To compare the results obtained from long- and short-time averages, Fig. 10 presents the lift and drag coefficients vs the angle of attack. The solid curves are the long-time averages of the 2-Hz data (all 76 runs), and the symbols are the 2-Hz data selected from six individual runs separated by about 10 deg to cover the entire range of angles of attack. The two symbols, circles and triangles, are alternated to demonstrate the range of short-time average angles of attack, α, covered by each run. It is evident that the vertical spread of the short-time-averaged data increases near and beyond dynamic stall. Both the long- and short-time averages behave surprisingly well with few exceptions. A similar behavior is observed in the plot of C_M vs α (not shown). The short-time averages do not show pronounced hysteresis loops, which are characteristic of their steady WT counterparts. The negative C_D corresponds to momentary net propulsion induced by the unsteady wind field, which becomes evident from the short-time averages. Again, according to Wu,[21] a wing undergoing a plunging oscillation rather than pitching is more efficient in thrust generation, particularly for low reduced frequencies.

Concluding Remarks

The results of the field experiments clearly demonstrate that atmospheric turbulence in the boundary layer has significant but favorable effects on the performance of the Wortmann wing. The aerodynamic characteristics of the Wortmann wing operating in the atmospheric boundary layer differ con-

siderably from those of its wind-tunnel counterpart under steady conditions. The importance of the unsteady effects is demonstrated by significant lift overshoot near and beyond the static stall angle, noticeable stall delay, and large reduction in the drag coefficient at small angles of attack in the full-scale results. Laboratory evidence indicates that the increase in C_L for an airfoil undergoing a plunging motion is larger than that for the same airfoil undergoing a pitching motion. The vortex-like disturbance initiated at the leading edge is thinner, longer, and less organized, and it moves downwind slower for a plunging airfoil than it does for a pitching airfoil. As a result, a high lift coefficient after passing the static stall angle could be sustained for a relatively long period of time, leading to a high mean lift coefficient averaged over many plunging cycles. In a turbulent wind field, the plunging motion experienced by the wing is definitely not of a single frequency, but is distributed over a wide range of frequencies depending on the spectrum of the wind field. The cumulative effect could well be a further increase in the lift coefficient.

The value of $C_{D\min}$ for R_c = 250,000–450,000 is also considerably lower for the FS data than for the wind-tunnel data. This is consistent with the analysis that the hydrodynamic efficiency is higher for the plunging oscillation than for the pitching motion, particularly at low reduced frequencies. Outside the minimum C_D region, as α_0 increases up to the stall onset point ($\alpha_0 \simeq 14$ deg), the region is characterized by a maximum unsteady lift that can be obtained with no significant penalty in pitching moment and drag. The combination of the high C_L and/or low C_D significantly increases the aerodynamic performance ratios L/D and $C_L^{3/2}/C_D$, as shown in Fig. 11. Further increases in the angle of attack will cause the wing to enter the light stall and deep stall regimes, in which both unsteady lift and drag increase; the increase in the drag is due to the induced drag. This also leads to a rapid decrease in the pitching moment. As a result of the fluctuating wind field, the aerodynamic coefficients do not show pronounced hysteresis loops, which are characteristic of their steady wind-tunnel counterparts.

The same trend was observed for another series of results with Reynolds numbers ranging from 80,000 to 200,000. As a result of low wind speeds and high turbulence intensity, the data scatter is relatively large for that set of data. For $R_c <$ 100,000, wind-tunnel results under steady conditions have indicated very peculiar aerodynamic behavior. It will be interesting to see how much the unsteadiness of the wind field can modify such behavior.

Acknowledgments

This work was sponsored by the U.S. Office of Naval Research under Contract N00014-85-C-0214 and by an IR&D fund from QUEST. The paper is revised from an article in the 1986 proceedings of the Low-Reynolds-Number Conference held at the Royal Aeronautical Society, London. The author would like to thank Paul Tacheron for his assistance in carrying out the field experiments and in the maintenance of the EATS. Special thanks are also due Ed Geller, Mort Cooper, and W.-H. Jou for their active participation in this project. They have provided many invaluable suggestions throughout the course of the investigation.

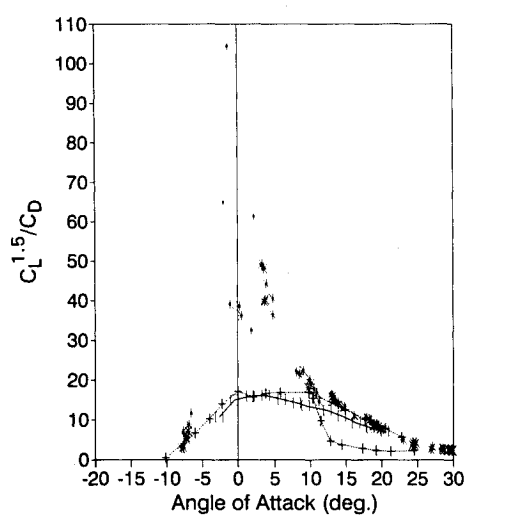

Fig. 11 Comparison of $C_L^{3/2}/C_D$ as a function of the angle of attack.

References

[1]McCroskey, W. J., "Unsteady Airfoils," *Annual Review of Fluid Mechanics*, Vol. 14, 1982, pp. 285–311.

[2]Chen, S.-H., "The Unsteady Aerodynamics of Plunging Airfoil," Ph.D. Dissertation, Aerospace Engineering, Univ. of Southern California, Los Angeles, CA, 1985.

[3]Maresca, S., Favier, D., and Rebont, J., "Unsteady Aerodynamics of an Airfoil at High Angle of Incidence Performing Various Linear Oscillations in a Uniform Stream," Paper 12, Fifth European Rotorcraft and Powered Lift Aircraft Forum, Amsterdam, Netherlands, 1979.

[4]Hamad, G., and Atassi, H., "Aerodynamic Response of an Airfoil with Thickness to a Longitudinal and Transverse Periodic Gust," AIAA Paper 80-0151, 1980.

[5]St. Hilaire, A. O., Carta, F. O., and Jepson, W. D., "The Influence of Sweep on the Aerodynamic Loading of an Oscillating NACA 0012 Airfoil," AHS Preprint 79-4, 1979.

[6]Liu, H.-T., Geller, E. W., and Cooper, M., "An Environmental Aerodynamic Test System for Low-Reynolds-Number Applications," *Proceedings of the Conference on Low Reynolds Number Airfoil Aerodynamics*, Univ. of Notre Dame, Notre Dame, IN, June 1985, pp. 207–218.

[7]Liu, H.-T., "Atmospheric Turbulence and Gust on the Performance of a Wortmann FX 63-137 Wing," *Proceedings of the Conference on Low-Reynolds-Number Aerodynamics*, Royal Aeronautic Society, London, UK, Oct. 1986.

[8]Mueller, T. J., "Low Reynolds Number Vehicles," AGARDograph 288, Feb. 1985.

[9]Bastedo, W. G. Jr., and Mueller, T. J., "Performance of Finite Wings at Low Reynolds Numbers," *Proceedings of the Conference on Low Reynolds Number Airfoil Aerodynamics*, Univ. of Notre Dame, Notre Dame, IN, June 1985, pp. 195–205.

[10]Marchman, J. F. III, Abtahi, A. A., and Sumantran, V., "Aspect Ratio Effects on the Aerodynamics of a Wortmann Airfoil at Low Reynolds Numbers," *Proceedings of the Conference on Low Reynolds Number Airfoil Aerodynamics*, Univ. of Notre Dame, Notre Dame, IN, June 1985, pp. 183–193.

[11]Althaus, D., *Profilpolaren fur den Modellflug*, N. V. Neckar Verlag Villingen-Schwenningen, 1980.

[12]Marchman, J. F. III, Sumantran, V., and Schaefer, C. G., "Acoustic and Turbulence Influences on Stall Hysteresis," AIAA Paper 86-0170, 1986.

[13]Pohlen, L. J., and Mueller, T. J., "Boundary Layer Characteristics of the Miley Airfoil at Low Reynolds Numbers," AIAA Paper 83-1795, 1983.

[14]Ho, C.-M., "An Alternative Look at the Unsteady Separation Phenomenon," *Symposium on Recent Advances in Aerodynamics and Aeroacoustics*, Stanford Univ., CA, Aug. 1983.

[15]McCroskey, W. J., "The Phenomenon of Dynamic Stall," NASA Technical Memorandum 81264, Ames Research Center, Moffett Field, CA, March 1981.

[16]Carta, F. O., "A Comparison of the Pitching and Plunging Response of an Oscillating Airfoil," NASA CR 3172, Oct. 1979.

[17]McCroskey, W. J., "Some Current Research in Unsteady Fluid Dynamics," *Journal of Fluids Engineering*, Vol. 99, 1977, pp. 8–38.

[18]Koochesfahani, M. M., "Vortical Patterns in the Wake of an Oscillating Airfoil," *AIAA Journal*, Vol. 27, 1989, pp. 1200–1205.

[19]Wu, J. C., and Singh, J., "Unsteady Aerodynamics of Non-Rigid Bodies—A Novel Approach," AIAA Paper 88-0565, 1988.

[20]Von Karman, T., and Burgers, J. M., "General Aerodynamic Theory—Perfect Fluids," *Aerodynamic Theory*, Division E, Vol. II, edited by W. F. Durand, 1943.

[21]Wu, T. Y., "Hydrodynamics of Swimming of Fishes and Cetaceans," *Advances in Applied Mechanics*, Vol. II, 1971, pp. 1–63.

[22]Liu, H.-T., "Unsteady Aerodynamics of a Wortmann FX-63-137 Wing in a Fluctuating Wind Field," Flow Research Rept. 431, Flow Research, Inc., Kent, WA, Nov. 1987.